

CHAPTER 6

MEASUREMENT OF $^{232}\text{Th}(n,\gamma)$ AND $^{238}\text{U}(n,\gamma)$ REACTION CROSS-SECTIONS USING ACTIVATION TECHNIQUE

6.1 Introduction

6.2 Experimental method

6.3 Data analysis

6.3.1 Calculation of neutron energy, flux and $^{232}\text{Th}(n,\gamma)$ and $^{238}\text{U}(n,\gamma)$ reaction cross-sections

6.3.2 Co-variance analysis

6.4 Result and discussion

6.5 Conclusion

References

Publication related to this chapter:

S. Mukherjee, Vibha Vansola, Siddharth Parashari, R. Makwana, N. L. Singh, S. V. Suryanarayana, S. C. Sharma, B. K. Nayak, H. Naik
Measurement of ^{232}Th and ^{238}U neutron capture cross-sections in the energy range 5–17 MeV
Applied Radiation and Isotopes 143 (2019) 72-78.

6.1 Introduction

^{232}Th is the only isotope for natural thorium and hence possesses 100% abundance, whereas ^{234}U , ^{235}U and ^{238}U are the three isotopes for natural uranium having abundances 0.006%, 0.71% and 99.3% respectively. Among all these isotopes ^{232}Th and ^{238}U are fertile materials and can be transformed into fissile materials so that they can be used as a fuel of a nuclear reactor [1-4]. This is a novel concept amongst all in the field of research for developing an advanced reactor. This advanced reactor technology will enable us to produce power with the challenge of nuclear waste disposal tackled in order to sustain the growth of nuclear energy for the future. Thorium and uranium fuel cycle with the right neutronics can address both the issues [3-38]. As shown in figure 1.2 in chapter 1, in thorium fuel cycle, the fertile host ^{232}Th gets converted into ^{233}U whereas; in uranium fuel cycle fertile host ^{238}U gets converted into ^{239}Pu . ^{233}U has a 2.47 times greater thermal neutron absorption cross-section than ^{232}Th . Thus Uranium is more likely to be used for the better conversion of fertile host into fissile material.

The above mentioned decay scheme figure 1.2 in chapter 1 shows that the generation of fissile nucleus ^{239}Pu is controlled by $^{238}\text{U}(n,\gamma)$ reaction cross-section and the generation of fissile nucleus ^{233}U is controlled by $^{232}\text{Th}(n,\gamma)$ reaction cross-section. In Accelerator driven sub-critical system (ADSs), the energy of neutrons is far greater than the typical reactors. Thus, reaction cross-sections for $^{232}\text{Th}(n,\gamma)$ and $^{238}\text{U}(n,\gamma)$ reactions at higher neutron energies cause considerable effect on the safety assessment and performance of ADSs and fast reactors. For India, which has abundant reserves of thorium, ADSs is quite advantageous in order to fully exploit its potential for designing the hybrid reactor systems, which are capable of producing the nuclear power with the help of thorium as the primary fuel [3, 39]. In ADSs, the fast neutrons will interact with the materials of the reactor and will cause different reactions. Thus, nuclear data such of reaction and fission cross-sections for all the materials playing an active and passive part such as fuel elements, structural materials and cladding materials at medium as well as fast neutron energies possess so much significance for designing the different types of reactors.

Significant amount of experimental data for Th and U cycles are available for neutron induced fission and reactions of structural materials and actinides at low energy and are available on EXFOR database [9]. An extended energy region can be explored for the construction of Accelerator driven sub-critical systems (ADSs). Nuclear data with higher accuracy for fission yields, neutron capture cross-sections, fission cross-sections and decay data, like half-lives, γ -ray energies, branching ratio, etc. are required for many advanced

reactor calculations. However, the measured data for mono-energetic neutron-induced fission and reaction of actinides in the medium (5-20 MeV) to high energy region are limited [9]. In addition to the above, almost all the nuclear data for the neutron induced fission of actinides available in the literature are based on an average neutron spectrum of the reactor. Also for the $^{232}\text{Th}(n,\gamma)$ reaction cross-sections are also predominantly based on the physical measurements and activation technique within thermal to 2.45 MeV and at 14.6 MeV neutron energy ranges [35, 13]. However, the experimental datum at 14.6 MeV neutron energy depends on D-T neutron source [35] and is notably higher than the expected value. All the available experimental $^{232}\text{Th}(n,\gamma)$ reaction cross-section data were measured by different authors [2, 5, 21, 26, 27, 38] and were found to be within the neutron energies of 3 MeV to 17.28 MeV, except for the datum at the neutron energy of 14.6 MeV [35]. There are no data available between 3.7 MeV to 5.9 MeV neutron energies. Whereas, for the $^{238}\text{U}(n,\gamma)$ reaction, adequate cross-section data are available in the literature [1, 7, 11, 15, 17, 18, 28, 32, 33, 35, 37] for a wide range of neutron energies. Below 8 MeV neutron energy, cross-section data are available from old work [1, 17, 18, 31, 32], which are notably higher than the theoretical results. Likewise, above 14 MeV neutron energy, the $^{238}\text{U}(n,\gamma)$ reaction cross-section data measured by the authors [32, 33, 35], are quite higher than the computed values. These remarks were made after the comparison and qualitative study of the similar data within the neutron energies of 2.45-17.3 MeV [1, 6, 11, 22, 24, 28, 37].

In the present work, I intend to do the further investigation on the above aspects with the help of the experiments of the neutron absorption cross-sections for ^{232}Th and ^{238}U in the fast neutron energy region. Since the possibility of the production and propagation of error is high, a detailed co-variance analysis was done in order to study how error is propagating from various quantities into the final experimental cross-sections [40-44]. In the present study, I have calculated excitation functions of the $^{232}\text{Th}(n,\gamma)$ and $^{238}\text{U}(n,\gamma)$ reactions with the help of computation code TALYS-1.9 [14]. Both the measured and computed values of reaction cross-section in the present work were compared with the measured [9] as well as evaluated data of the ENDF/B-VII-1 [9] and JENDL-4.0 [40] nuclear data libraries.

6.2 Experimental method

The 14UD Bhabha Atomic Research Centre-Tata Institute of Fundamental Research (BARC-TIFR) Pelletron Facility in Mumbai, India was used to carry out the present experiments [19, 27, 28, 38]. The $^7\text{Li}(p, n)$ reaction was used for the generation of the quasi mono-energetic neutron beam at high energies. For this purpose, proton beams having

different energies from the main line at Pelletron facility having 6-meter height above the analyzing magnet was used. For proton beam, 50-90 keV energy spread was observed at this port. In order to regulate the terminal voltage by generating voltage mode (GVM), a terminal potential stabilizer was used at this port. Here, quasi mono-energetic neutrons were generated, which were further used to irradiate the targets of the fertile elements (^{232}Th and ^{238}U). These fertile elements are of immense importance in development of advanced reactors and ADSs. Lithium foil (Natural) having the thickness of 8.0 mg/cm^2 placed between two tantalum foils having different thicknesses. The thickness of the front tantalum foil was 3.7 mg/cm^2 . It was made to face the proton beam, whereas, a Ta foil having the thickness of 4.12 mg/cm^2 was kept at the back side to reduce the energy of the proton beam. SRIM code [44] was used for calculating the degradation of the proton beam in the Ta-Li-Ta stack. The proton energy values at the centre of the Li target were used to calculate the effective neutron energies. Th and U samples were kept behind the Ta-Li-Ta stack. Natural ^{232}Th and ^{238}U metal foil samples had thickness of 0.025 mm and area $1 \times 1 \text{ cm}^2$. All the samples were wrapped with aluminium foil having thickness of 0.025 mm (purity > 99.99%). The aluminium wrapping was done for stopping and collecting the fission products, which were recoiling out from the surface of the samples and for avoiding the radioactive contamination of other samples and surrounding materials. The ^{232}Th and ^{238}U samples were mounted at 2.1 cm distance from the Ta-Li-Ta stack. A schematic diagram showing the activation set up is shown in figure 2.2 in chapter 2.

Four different sets of samples were prepared for each irradiation with different neutron energies. The irradiations were done at the proton energies (E_p) of 7, 11, 15 and 18.8 MeV. All the details regarding the irradiation of each sample is given in Tables 6.1 and 6.2. After the irradiation, the activated samples were cooled for some time. After the cooling, activated samples along with Al wrapper were mounted on different Perspex plates with the help of forceps. These mounted samples were kept in front of the HPGe detector for γ -ray spectrometry.

Energy and efficiency calibrated 80 cm^3 HPGe detector coupled with a PC-based 4K channel analyzer was used for counting of the γ -rays of fission/reaction products from the irradiated Th and U samples. During the counting of the samples, the resolution of the detector was measured as 2.0 keV at 1332 keV of ^{60}Co . Activated Th and U samples were kept at a certain distance from the detector head for avoiding the pileup effects, and hence, the counting dead time of the detector less than 2%. The standard ^{152}Eu multi γ -ray source was used for the energy and the efficiency calibration of the detector system. According to

the half-life of the irradiated samples, the γ -ray counting of the activated Th and U samples was repeated over an extended period for reducing the statistical error. Recorded γ -ray spectra of the irradiated Th and U samples are shown in figures 6.1 and 6.2.

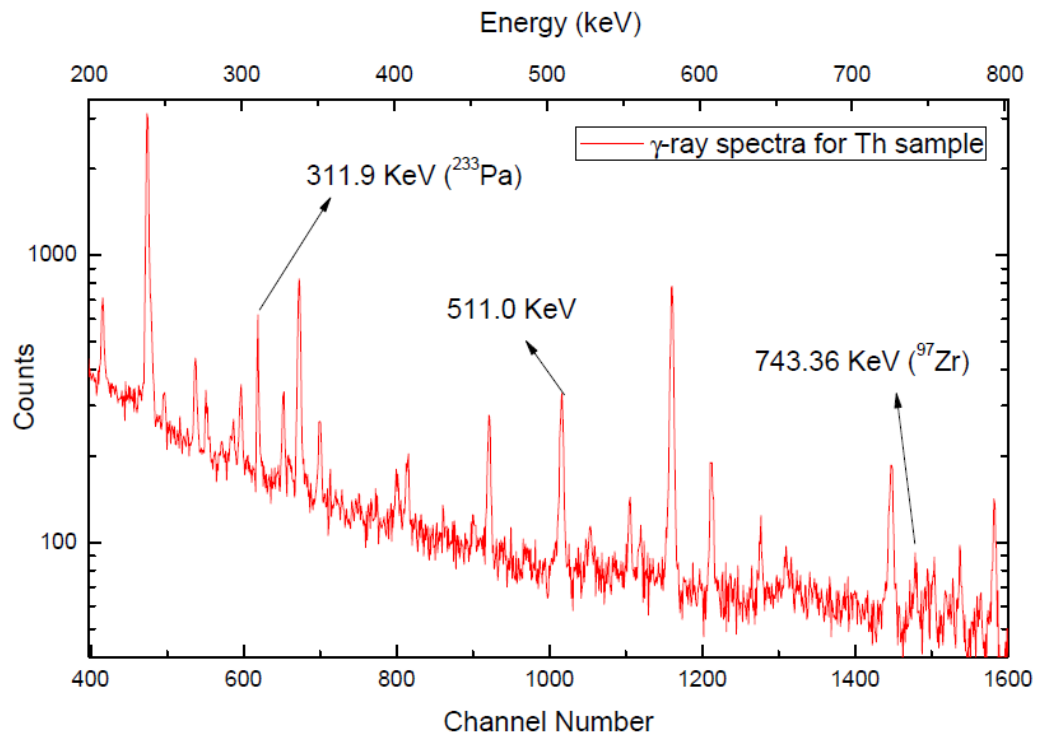


Figure 6.1: γ -ray spectrum from the irradiated sample of ^{232}Th at 18.8 MeV

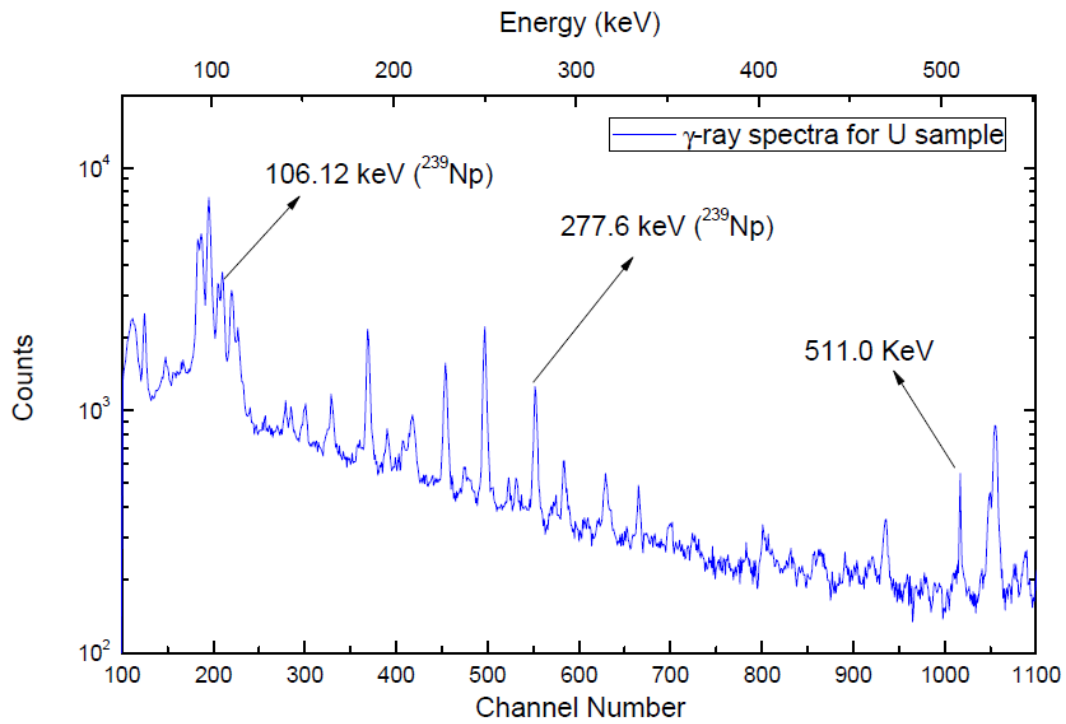


Figure 6.2: γ -ray spectrum from the irradiated sample of ^{238}U at 18.8 MeV

Table 6.1: Details of the thorium and uranium irradiations

	Irradiation -1	Irradiation-2	Irradiation-3	Irradiation-4
Proton energy (MeV)	18.8	7.0	15.0	11.0
Irradiation time (h:min)	5:00	11:15	7:00	16:05
Proton beam current (nA)	140	100	135	150
Thorium weights (g)	0.1955	0.1911	0.1907	0.1905
Uranium weights (g)	0.3127	0.2995	0.2884	0.4473

Table 6.2: Selected reactions, half life of product, Q value and threshold of reaction

Reaction	Half life	Q-Value (keV)
$^{238}\text{U}(n,\gamma)^{239\text{g}}\text{U}$	23.45m	4806.38±0.17
$^{232}\text{Th}(n,\gamma)^{233\text{g}}\text{Th}$	22.3m	4786.39±0.09

6.3 Data analysis

6.3.1 Calculation of neutron energy, flux and $^{232}\text{Th}(n,\gamma)$ and $^{238}\text{U}(n,\gamma)$ reaction cross-sections

Accuracy in flux measurement helps in the measurement of cross-section, precisely. In the present work, ^{232}Th and ^{238}U were used as the target isotopes for the determination of $^{232}\text{Th}(n,\gamma)$ and $^{238}\text{U}(n,\gamma)$ reaction cross-sections. For the determination of the neutron flux incident on the target, the fission reaction $^{232}\text{Th}(n, f)$ was considered as a flux monitor in the present work. Similar procedure was followed in one of our publication [19]. Also the neutron spectra used for flux measurement, were taken from our previous work [19]. Table 6.3 shows the spectroscopic data, which was used for the measurements of flux and reaction cross-section and were taken from NuDat [29]. The ^{97}Zr isotope is generated as a fission product, in the fission of ^{232}Th . This ^{97}Zr has a half-life of 16.749 ± 0.008 h [29]. The photo-peak area of 743.36 keV [29] γ -ray estimates the production of ^{97}Zr isotope. The fission yields of ^{97}Zr are known from our previous publications [23, 25] and are given in tables 6.3. Thus, one can evaluate the neutron flux with the help of neutron activation analysis (NAA) technique. The neutron flux (Φ) incident on the target was estimated with the help of following equation:

$$\Phi = \frac{A_{obs} \frac{CL}{LT} \lambda}{NY \langle \sigma_f \rangle I_\gamma \varepsilon (1 - e^{-\lambda T_i}) e^{-\lambda T_c} (1 - e^{-\lambda CL})} \quad (6.1)$$

Where, N is the number of target atoms, Y is yield of fission product [23, 25] and σ_f is the spectrum averaged fission cross-section. EXFOR database [9] contains the fission cross-sections at wide range of neutron energies. Decay constant of the product of interest having a half-life, $T_{1/2}$ is denoted by λ ($\lambda = \ln 2/T_{1/2}$). I_γ is the branching intensity of ^{97}Zr at 743.36 keV γ -line of and ε is the detector efficiency. T_i , T_c , CL and LT are the irradiation time, cooling time, real time and live time, respectively.

Eq. (6.1) is used to calculate the neutron flux (Φ) and are given in Tables 6.7 and 6.8. The $^{232}\text{Th}(n,\gamma)$ and $^{238}\text{U}(n,\gamma)$ reaction cross-sections (σ_R) were calculated with the help of the rearranged equation of cross-section, with the γ -ray photo-peak activities of ^{233}Pa and ^{239}Np . Both the equations hold the same significance and all the terms hold the same meaning as in Eq. (6.1). For calculating the $^{232}\text{Th}(n,\gamma)$ and $^{238}\text{U}(n,\gamma)$ reaction cross-sections, the neutron flux (Φ) from Tables 6.7 and 6.8 were used. The necessary nuclear spectroscopic input data for the calculations were taken from the literature [29].

The low energy tail part has a significant contribution in the $^{232}\text{Th}(n,\gamma)$ and $^{238}\text{U}(n,\gamma)$ reactions cross-section values, and hence, the contribution coming from the tail part of the

neutron should be subtracted from the measured cross-sections. This cross-section contribution for the $^{232}\text{Th}(n,\gamma)$ and $^{238}\text{U}(n,\gamma)$ reactions have been evaluated with the help of the calculation of the weighted average values from ENDF/B-VII.1 [9] and JENDL-4.0 [40]. This was done by folding the cross-sections with neutron flux distributions, which were taken from ref. [19]. A detailed discussion on tailing correction is provided in our previous publications [19, 27, 28, 38].

Table 6.3: Fission and reaction nuclides, with their half-lives, decay modes and related prominent γ -ray energies with branching intensities (NuDat). The γ -ray energies and branching intensities (abundances), marked with bold letters were used in the calculations [29].

Nuclide	Half-life	Decay mode	E_γ (keV)	I_γ (%)
$^{97}_{40}\text{Zr}$	16.749 ± 0.008 h	β^- (100 %)	355.40	2.09
			507.64	5.03
			743.36	93.09
			1147.97	2.62
$^{233}_{91}\text{Pa}$	26.975 ± 0.013 d	β^- (100 %)	311.9	38.5
			106.12	25.34
$^{239}_{93}\text{Np}$	2.356 ± 0.003 d	β^- (100 %)	209.75	3.363
			228.18	10.73
			277.6	14.51

6.3.2 Co-variance analysis

Here for the calculation of the flux for both the $^{232}\text{Th}(n,\gamma)$ and $^{238}\text{U}(n,\gamma)$ reactions, the $^{232}\text{Th}(n,f)^{97}\text{Zr}$ reaction cross-sections were used. An off-line γ -ray spectroscopic measurement was done for both the sample reactions with the help of a common pre-calibrated HPGe detector set up. Thus, both the sample reaction cross-sections are correlated with the monitor reaction cross-sections among the four neutron energies as well as with each other. Therefore, to find the degree of uncertainty in the measurement in the correlation coefficients for such a case, covariance analysis was used.

To normalize the measured cross-sections with monitor reaction cross-sections, the ratio measurement technique [41] was used. We have adopted the methodology demonstrated in the references [30, 41]. However, S_{ij} 's, which are known as the micro correlation matrices were modified carefully as the quantities used in the calculations, are correlated. A point source and the samples of a finite size were used to calibrate the HPGe detector therefore they possess a geometry effect on the experimentally calculated efficiencies of the detector. To incorporate the solid angle effect, EFFTRAN code [43] was used and the geometry and summing correction factors have been taken into the account. Tables 6.4 and 6.5 show the covariance matrix (V_{ij} 's) along with the correlation coefficients for the efficiencies and experimentally calculated cross-sections for monitor and sample reactions, respectively.

The product of tailing corrected cross-section with the square root of the diagonal element of the respective neutron energy ($\sqrt{V_{ij}} \times \sigma_R$) of the covariance matrix V_{ij} will give the error present in the measured cross-section. Table 6.6 shows the correlation coefficients for the measured cross-sections. The table was divided in four quadrants so that it can be easily understandable. The correlations for the $^{232}\text{Th}(n,\gamma)$ and $^{238}\text{U}(n,\gamma)$ reaction cross-sections among the four neutron energies are given in the first and fourth quadrant, respectively. The correlations of the $^{232}\text{Th}(n,\gamma)$ reaction cross-sections with the $^{238}\text{U}(n,\gamma)$ reaction cross-sections among the four neutron energies are given in the third quadrant. From the Table 6.6, it can be observed that the correlations are strongest (diagonal elements in the third quadrant) among the two sample reactions and weakest among the monitor and the $^{238}\text{U}(n,\gamma)$ reaction cross-sections, which is a result of using Th foils as monitor and sample calculations [34]. This is the reason why the significant correlations in the first quadrant are more than those given in the fourth quadrant. The calculated uncertainties with the measured cross-sections for the present work are given with the measured cross-sections for the present work in Tables 6.7 and 6.8.

Table 6.4: Covariance matrix for efficiencies used in the measurement

γ-ray energy (keV)	Covariance matrix	Correlation coefficients
277.6	1.45E-06	1
311.26	1.41E-06 1.48E-06	0.960 1
743.36	-1.1E-08 -3.5E-08 5.86E-08	-0.039 -0.118 1

Table 6.5: Covariance matrix for the measured cross-sections

En (MeV)	Reaction	Covariance matrix
5.08±0.17	Th (n, γ)	0.027033
8.96±0.77		0.003553 0.021786
12.47±0.83		0.003553 0.003553 0.038442
16.63±0.95		0.003553 0.003553 0.003553 0.025693
5.08±0.17	U (n, γ)	0.016901 0.002464 0.002464 0.002464 0.034921
8.96±0.77		0.002464 0.010303 0.002464 0.002464 0.001974 0.018471
12.47±0.83		0.002464 0.002464 0.015266 0.002464 0.001973 0.001976 0.027509
16.63±0.95		0.002464 0.002464 0.002464 0.010833 0.001973 0.001976 0.001974 0.018328

Table 6.6: Correlation matrix for the measured cross-sections

En (MeV)	Reaction	Correlation matrix									
5.08±0.17	Th (n, γ)	1.000									
8.96±0.77		0.146	1.000								
12.47±0.83		0.110	0.123	1.000							
16.63±0.95		0.135	0.150	0.113	1.000						
5.08±0.17	U (n, γ)	0.550	0.089	0.067	0.082	1.000					
8.96±0.77		0.110	0.514	0.092	0.113	0.078	1.000				
12.47±0.83		0.090	0.101	0.469	0.093	0.064	0.088	1.000			
16.63±0.95		0.111	0.123	0.093	0.499	0.078	0.107	0.088	1.000		

Table 6.7: Reaction cross-sections at different neutron energies for $^{232}\text{Th}(n, \gamma)$ reaction

Neutron energy (MeV)	^{97}Zr Fission Yields (%)	Spectrum averaged cross-section for $\text{Th}(n,f)$ monitor (mb)	Flux ($\text{n}/\text{cm}^2 \cdot \text{sec}$)	$^{232}\text{Th}(n, \gamma)$ reaction cross-section (mb)			
				Present work (mb)	TALYS-1.9 (mb)	ENDF (mb)	JENDL (mb)
5.08±0.17	4.639±0.42 (Naik et al., 2016)	99.0	1.06E+06	2.26 ±0.37	7.82	2.607	2.827
8.96±0.77	4.838±0.35 (Naik et al., 2016)	220.0	4.2E+06	1.46±0.21	1.07	0.881	1.204
12.47±0.83	4.672±0.33 (Naik et al., 2016)	270.0	1.11E+07	1.33±0.26	1.53	1.155	1.379
16.63±0.95	3.41±0.15 (Mukerji et al., 2014)	342.0	1.11E+07	0.78±0.12	0.754	0.356	0.642

Table 6.8: Reaction cross-sections at different neutron energies for $^{238}\text{U}(n, \gamma)$ reaction

Neutron energy (MeV)	^{97}Zr Yields (%)	Fission	Spectrum averaged		$^{238}\text{U}(n, \gamma)$ reaction cross-section (mb)			
			cross-section for Th(n,f) monitor (mb)	Flux (n/cm ² .sec)	Present work (mb)	TALYS-1.9 (mb)	ENDF (mb)	JENDL (mb)
5.08±0.17	4.639±0.42 (Naik et al., 2016)		99.0	1.06E+06	1.87±0.34	2.91	2.080	1.159
8.96±0.77	4.838±0.35 (Naik et al., 2016)		220.0	4.2E+06	1.17±0.16	1.00	0.653	1.096
12.47±0.83	4.672±0.33 (Naik et al., 2016)		270.0	1.11E+07	1.88±0.31	1.50	1.021	0.776
16.63±0.95	3.41±0.15 (Mukerji et al., 2014)		342.0	1.11E+07	0.75±0.10	0.737	0.455	0.313

6.4 Result and discussion

Tables 6.7 and 6.8 shows the tailing corrected measured cross-sections of the $^{232}\text{Th}(n,\gamma)$ and $^{238}\text{U}(n,\gamma)$ reactions, respectively. These values were obtained after removal of the contribution from the tail part of the neutron spectra. The covariance analysis was used for calculating the uncertainties associated with the measured $^{232}\text{Th}(n,\gamma)$ and $^{238}\text{U}(n,\gamma)$ reaction cross-sections. As stated in the introduction, there are some literature data available for the $^{232}\text{Th}(n,\gamma)$ [13, 27, 35, 38] and $^{238}\text{U}(n,\gamma)$ [1, 7, 11, 17, 18, 26, 28, 32, 33, 37] reactions, below the neutron energy of 3 MeV and within 13-15 MeV. These literature data are plotted along with the present experimental data as shown in Figs. 6.3 and 6.4 for the $^{232}\text{Th}(n,\gamma)$ and $^{238}\text{U}(n,\gamma)$ reactions, respectively. The data within the neutron energies of 5-7 MeV and within 17-20 MeV [1, 7, 15, 18, 32, 33] and also at 14.5 MeV [35] are higher than the present data. Whereas, the data of present work at the neutron energies of 8.96 ± 0.77 , 12.47 ± 0.83 and 16.63 ± 0.95 MeV are higher than the data reported by McDaniels et al. [20] around 9.2-14.2 MeV neutron energies. D+D and D+T neutron sources were used to measure the $^{238}\text{U}(n,\gamma)$ reaction cross-sections obtained by Panitkin et al., 1972 [32-33] within the neutron energies of 5-7 MeV and 17-20 MeV as well as by Perkin et al., 1958 [35] at 14 MeV. Contrary to this, the $^{238}\text{U}(n,\gamma)$ reaction cross-sections at higher neutron energies obtained by Perkin et al. [35] and Panitkin et al. [32-33] are results of the contributions of the scattered low energy neutrons.

For the investigation of these particulars, the $^{232}\text{Th}(n,\gamma)$ and $^{238}\text{U}(n,\gamma)$ reaction cross-sections in between neutron energies of 1 to 20 MeV were also computed theoretically with the help of computer code TALYS-1.9 [14] utilizing the default input parameters. The computer code TALYS-1.9 [14] is used for the prognostication and the study of nuclear reactions. TALYS-1.9 can be used as a computation tool, challenging nuclear models with experiment and also as a tool for the prognostication of the nuclear data. Simulation of nuclear reactions involving gammas, neutrons, protons, deuterons, tritons, ^3He and alpha-particles having the incident energy range from 1 keV to 200 MeV for target nuclides with mass 12 and heavier can be done by the TALYS-1.9 program. The present work represents the irradiation of the ^{232}Th and ^{238}U targets with the help of neutron of energies up to 20 MeV. Including inelastic and fission channels, all the possible outgoing channels for neutron as a projectile were taken into account. Although, the (n,γ) reaction cross-sections were considered specifically and collected. Figures 6.3 and 6.4 show the theoretically computed $^{232}\text{Th}(n,\gamma)$ and $^{238}\text{U}(n,\gamma)$ reaction cross-sections at 1 to 20 MeV neutron energies with the help of TALYS-1.9 code. Another data set of neutron induced reaction cross-sections at four

different neutron energies is measured for $^{232}\text{Th}(n,\gamma)$ reaction at four different neutron energies by Siddharth Parashari from our group [45]. In addition to this, the evaluated reaction cross-sections data for the $^{232}\text{Th}(n,\gamma)$ and $^{238}\text{U}(n,\gamma)$ reactions from the ENDF/B-VII.1 [9] and JENDL-4.0 [40] nuclear data libraries are also demonstrated in figures 6.3 and 6.4.

From Figs. 6.3 and 6.4, it is clear that the present data is following the trend of theoretically computed values using TALYS-1.9 code [14] and the evaluated data from the data library [9, 40]. Additionally, the computed [14], the evaluated [9, 40] and the present measured $^{232}\text{Th}(n,\gamma)$ and $^{238}\text{U}(n,\gamma)$ reactions cross-sections and literature data [1, 2, 4-8, 10-11, 13, 15-18, 20-22, 24, 26-28, 31-33, 35-38, 42] are observed to be declining from the neutron energy 0.025 eV to 6-7 MeV. Subsequently, the $^{232}\text{Th}(n,\gamma)$ and $^{238}\text{U}(n,\gamma)$ reaction cross-sections increase till 12 MeV and decrease afterwards. The reason behind this is the threshold values of (n,2n) reaction of the ^{232}Th and ^{238}U are 6.47 MeV and 6.18 MeV, respectively and hence the (n,2n) reaction starts to dominate all other reactions above 6.5 MeV neutron energy. Below 6 MeV neutron energy, the (n, γ) and (n,n') reaction cross-sections compete each other. Below 6 MeV neutron energy, the (n, γ) reaction cross-sections are three times smaller than the (n,n') reaction cross-sections. Beyond 7 MeV, (n,n') reaction cross-section becomes almost constant. Then the (n, γ) and (n,2n) reactions start to dominate, while the $^{232}\text{Th}(n,2n)$ and $^{238}\text{U}(n,2n)$ reaction cross-sections start dominating. The $^{232}\text{Th}(n,\gamma)$ and $^{238}\text{U}(n,\gamma)$ reaction cross-sections start decreasing around 6.5-7.5 MeV neutron energy. Also within 8 to 12 MeV neutron energies, the (n,2n) reaction cross-section becomes almost constant and the (n, γ) reaction cross-sections again increases. Further, as the neutron energy increases, new reaction channels open up, i.e., above 12-14 MeV neutron energies, both the (n, γ) and (n,2n) reaction cross-sections decrease due to the opening of (n,3n) channel, which has a threshold value of 11.33 MeV for the ^{238}U and 11.61 MeV for ^{232}Th isotope. Hence, the observed pattern of the (n, γ) and (n,2n) reaction cross-sections can be explained by the sharing of energy for both the ^{232}Th and ^{238}U isotopes.

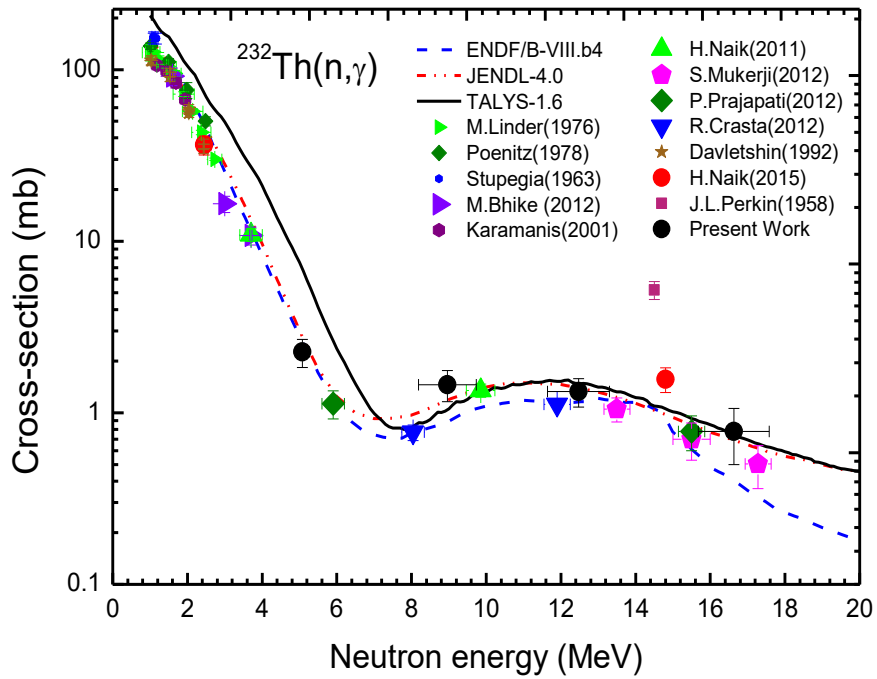


Figure 6.3: Comparison of present measured $^{232}\text{Th}(n,\gamma)$ reaction cross-section with the measured data available in the literature, computed values from TALYS-1.9 and evaluated data of ENDF/B-VII.1 and JENDL-4.0

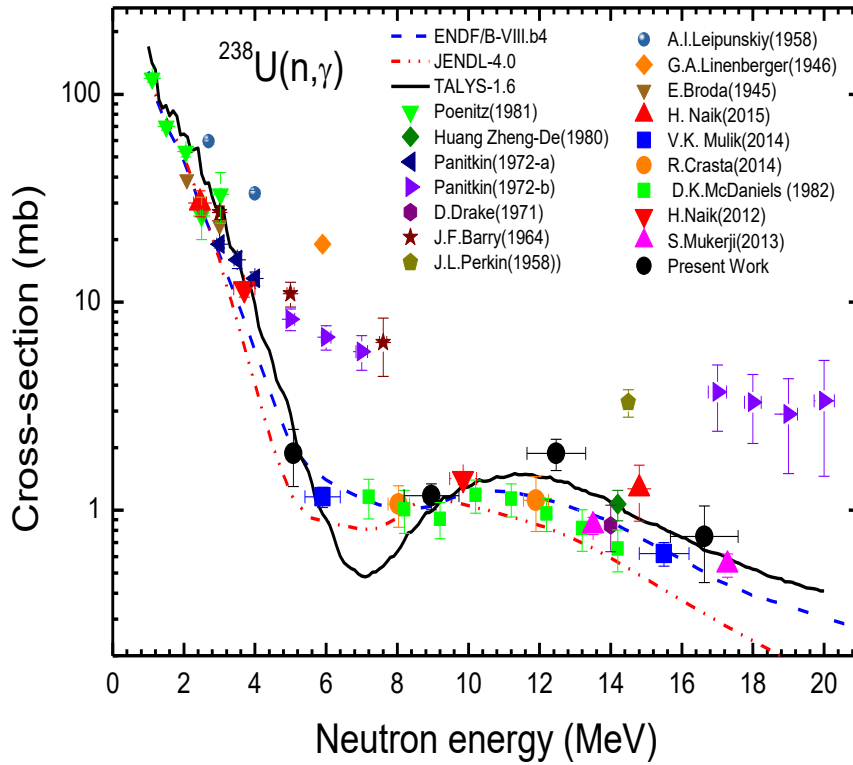


Figure 6.4: Comparison of present measured $^{238}\text{U}(n,\gamma)$ reaction cross-section with the measured data available in the literature, computed values from TALYS-1.9 and evaluated data of ENDF/B-VII.1 and JENDL-4.0

6.5 Conclusion

The present measured cross-section data for both the $^{232}\text{Th}(n,\gamma)$ and $^{238}\text{U}(n,\gamma)$ reactions hold so much importance from the advanced nuclear reactor technology view point; nuclear reactor waste transmutation and for more efficient and accurate nuclear data generation for bettering the present reactor technology. In thorium and uranium fuel cycles, one can see that the generation of fissile nucleus ^{239}Pu is controlled by $^{238}\text{U}(n,\gamma)$ reaction cross-section and the generation of fissile nucleus ^{233}U is controlled by $^{232}\text{Th}(n,\gamma)$ reaction cross-section. Furthermore, in ADSs, the neutron energy is far greater than that of the neutrons in typical reactors. Thus, there is a strong need of reaction cross-section data for $^{232}\text{Th}(n,\gamma)$ and $^{238}\text{U}(n,\gamma)$ reactions at higher neutron energies. For India, which has considerable amount of reserves of thorium, ADSs is of a great use. In ADSs, the fast neutrons will interact with the materials of the reactor and will cause different reactions. Thus, nuclear data such as reaction and fission cross-sections of all the materials playing active and passive part such as fuel elements, structural materials and cladding materials at medium as well as fast neutron energies possess so much significance for designing the different types of reactors.

Neutron activation analysis and off-line γ -ray spectrometric technique was used to measure the $^{232}\text{Th}(n,\gamma)$ and $^{238}\text{U}(n,\gamma)$ reaction cross-sections at the average neutron energies of 5.08 ± 0.17 , 8.96 ± 0.77 , 12.47 ± 0.83 and 16.63 ± 0.95 MeV. Covariance analysis was applied to calculate the uncertainties present in the measured cross-section data and were found to be in between 13-20%. I have also computed the $^{232}\text{Th}(n,\gamma)$ and $^{238}\text{U}(n,\gamma)$ reaction cross-section data using the TALYS-1.9 code. Both, the present measured as well as computed cross-section data for $^{232}\text{Th}(n,\gamma)$ and $^{238}\text{U}(n,\gamma)$ reactions were compared with the evaluated data available in ENDF/B-VII-1 and JENDL-4.0 nuclear data libraries as well as with the literature data taken from the EXFOR data library and were found in a fairly good agreement.

References

- [1] J. F. Barry, J. Bunce, P. H. White, *J. Nucl. Energy AB React. Sci. Technol.* **18**, 481 (1964).
- [2] M. Bhike, B. J. Roy, A. Saxena, R. K. Choudhury, S. Ganesan, *Nucl. Sci. Eng.* **170**, 44 (2012).
- [3] C. D. Bowman, *Annu. Rev. Nucl. Part. Sci.* **48**, 505 (1998).
- [4] E. Broda, *Cavendish Lab. Reports No.* **574** (1945).
- [5] R. Crasta, H. Naik, S. V. Suryanarayana, B. S. Shivashankar, V. K. Mulik, P. M. Prajapati, G. Sanjeev, S. C. Sharma, P. V. Bhagwat, A. K. Mohanty, S. Ganesan, A. Goswami, *Ann. Nucl. Energy* **47**, 160 (2012).
- [6] R. Crasta, S. Ganesh, H. Naik, A. Goswami, S. V. Suryanarayana, S. C. Sharma, P. V. Bhagwat, B. S. Shivashankar, V. K. Mulik, P.M. Prajapati, *Nucl. Sci. Eng.* **178**, 66–75 (2014).
- [7] D. Drake, I. Bergqvist, D. K. Mcdaniels, *Phys. Lett. B* **36**, 557 (1971).
- [8] A. N. Davletshin, E. V. Teplov, A. O. Tipunkov, V. A. Tolstikov, I. A. Korzh, V. D. Ovdienko, N. M. Pravdivyy, N. T. Sklyar, V. A. Mishchenko, A. N. Davletshin, *Vop. At. Nauki i Tekhn. Ser. Yad. Konstant.* 41 (1992).
- [9] ENDF/B-VII.1, National Nuclear Data Center, Brookhaven National Laboratory, (2011). <http://www.nndc.bnl.gov/exfor/endl00.jsp>.
- [10] R. C. Hanna, B. Rose, *J. Nucl. Energy* **8** (4), 197–205 (1959).
- [11] Huang Zheng-De, Cao Zhong, Hui-Zhu, Wang, Ji-Shi, Liu, Da-Zhao, Ding, Lawrence Berkeley Lab. 243 (Reports No.11118) (1980).
- [12] IAEA-TECDOC-1319 Fast Reactors and Accelerator Driven Systems Knowledge Base, Thorium fuel utilization: Options and Trends (2002).
- [13] D. Karamanis, M. Petit, S. Andriamonje, G. Barreau, M. Bercion, A. Billebaud, B. Blank, S. Chajkowski, V. Lacoste, C. Marchand, R. DelMoral, J. Giovinazzo, L. Perrot, M.Pravikoff, J. C. Tomas, *Nucl. Sci. Eng.* **139**, 282 (2001).
- [14] A. J. Koning, S. Hilaire, S. Goriely. TALYS User Manual: A Nuclear Reaction Program. NRG, ZG PETTEN, The Netherlands, 1755 (2015).
- [15] A. I. Leipunskiy, O. D. Kazachkovskiy, G. J. Artyukhov, A. I. Baryshnikov, T. S. Belanova, V. I. Galkov, Yu. Ja. Stavisskiy, E. A. Stumbur, L. E. Sherman, *Second Internat. At. En. Conference, Geneva* **15**, 50 (1958).
- [16] M. Lindner, R. J. Nagle, J. H. Landrum, *Nucl. Sci. Eng.* **59**, 381 (1976).

- [17] D. Linenberger, G. A. Miskel, J. Segre, E. Bailey, C. Blair, J. Frisch, D. Greene, K. Greisen, A. O. Hanson, Hush, E. Klema, R. Krohn, R. Perry, W. Seagondollar, W. D. Smith, R. Taschek, C. Turner, 1944. Los Alamos Scientific Lab. Reports No. 137.
- [18] G. A. Linenberger, J. A. Miskel, Los Alamos Scientific Lab. Reports, No.467 (1946).
- [19] R. Makwana, S. Mukherjee, P. Mishra, H. Naik, N. L. Singh, M. Mehta, K. Katovsky, S. V. Suryanarayana, V. Vansola, Y. S. Sheela, M. Karkera, R. Acharya, S. Khirwadkar, Phys. Rev. C **96**, 024608 (2017).
- [20] D. K. McDaniels, P. Varghese, D. M. Drake, E. Arthur, A. Lindholm, I. Bergqvist, J. Krumlinde, Nucl. Phys. A **384**, 88 (1982).
- [21] S. Mukerji, H. Naik, S. V. Suryanarayana, S. Chachara, B. S. Shivasankar, V. K. Mulik, R. Crasta, S. Samanta, B. K. Nayak, A. Saxena, S. C. Sharma, P. V. Bhagwat, K. K. Rasheed, R. N. Jindal, S. Ganesan, A. K. Mohanty, A. Goswami, P. D. Krishani, Pramana **79** (2), 249 (2012).
- [22] S. Mukerji, H. Naik, S. V. Surayanarayana, B. S. Shivashankar, V. K. Mulik, Chachara, Sachin, Samanta, Sudipta, A. Goswami, P. D. Krishnani, J. Basic Appl. Phys. **2**, 104 (2013).
- [23] S. Mukerji, H. Naik, S. V. Suryanarayana In: Proceedings of the DAE Symposium on Nuclear Physics **59**, 426 (2014).
- [24] V. K. Mulik, S. V. Surayanarayana, H. Naik, Sadhana Mukherji, B. S. Shivashankar, P. M. Prajapati, S. D. Dhole, V. N. Bhoraskar, S. Ganesan, A. Goswami, Ann. Nucl. Energy **63**, 233 (2014).
- [25] H. Naik, S. Mukherji, S. V. Suryanarayana, K. C. Jagadeesan, S. V. Thakare, S. C. Sharma, Nucl. Phys. A **952**, 100 (2016).
- [26] H. Naik, S. V. Surayanarayana, S. Bishnoi, T. Patel, A. Sinha, A. Goswami, J. Radioanal. Nucl. Chem. **303**, 2497 (2015).
- [27] H. Naik, P. M. Prajapati, S. V. Surayanarayana, K. C. Jagadeesan, S. V. Thakare, D. Raj, V. K. Mulik, B. S. Sivashankar, B. K. Nayak, S. C. Sharma, S. Mukherjee, S. Singh, A. Goswami, S. Ganesan, V. K. Manchanda, Eur. Phys. J. A **47**, 51 (2011).
- [28] H. Naik, S. V. Suryanarayana, V. K. Mulik, P. M. Prajapati, B. S. Shivashankar, K. C. Jagadeesan, S. V. Thakare, D. Raj, S. C. Sharma, P. V. Bhagwat, S. D. Dhole, V. N. Bhoraskar, A. Goswami, Radioanal. Nucl. Chem. **293**, 469 (2012).
- [29] NuDat 2.7 β , National Nuclear Data Center, Brookhaven National Laboratory. (<http://www.nndc.bnl.gov/>).
- [30] N. Otuka, B. Lalremruata, M. U. Khandaker, A. R. Usmand, L. R. M. Punte, Radiat. Phys. Chem. **140**, 502–510 (2017).

- [31] Yu. G. Panitkin, Yu. Ya. Stavisskiy, V. A. Tolstikov, Neutron Physics Conference, Kiev **1**, 321 (1971).
- [32] Yu. G. Panitkin, V. A. Tolstikov, Sov. At. Energy **33**, 893 (1972a).
- [33] Yu.G. Panitkin, V. A. Tolstikov, Sov. At. Energy **33**, 945 (1972b).
- [34] Siddharth Parashari, S. Mukherjee, S. V. Suryanarayana, B. K. Nayak, Rajnikant Makwana, N. L. Singh and H. Naik, Phys. Rev. C **99**, 044602 (2019).
- [35] J. L. Perkin, L. P. O`connor, R. F. Coleman, Proc. Phys. Soc. (Lond.) **72**, 505 (1958).
- [36] W. P. Poenitz, D. L. Smith, Argonne National Laboratory Reports No. 42 (1978).
- [37] W. P. Poenitz, Nucl. Sci. Eng. **57**, 300 (1975).
- [38] P. M. Prajapati, H. Naik, S. V. Suryanarayana, S. Mukherjee, K. C. Jagadeesan, S. C. Sharma, S. V. Thakre, K. K. Rasheed, S. Ganesan, A Goswami, Eur. Phys. J. A **48**, 35 (2012).
- [39] C. Rubbia, J. A. Rubio, S. Buono, F. Carminati, N. Fietier, J. Galvez, C. Geles, Y. Kadi, R. Klapisch, P. Mandrillon, J. P. Revol, C. H. Roche, CERN Report No. CERN/AT/95-44 (ET) (1995).
- [40] K. Shibata, O. Iwamoto, T. Nakagawa, N. Iwamoto, A. Ichihara, S. Kunieda, S. Chiba, K. Furutaka, N. Otuka, T. Ohasawa, T. Murata, H. Matsunobu, A. Zukeran, S. Kamada, JENDL-4.0: a new library for nuclear science and engineering. J. Nucl. Sci. Technol. **48** (2011).
- [41] B. S. Shivashankar, S. Ganesan, H. Naik, S. V. Suryanarayan, N. S. Nair, K. M. Prasad, Nucl. Sci. Eng. **179** (4), 423–433 (2015).
- [42] D. C. Stupegia, A. B. Smith, K. Hamm, J. Inorg. Nucl. Chem. **25**, 627 (1963).
- [43] T. Vidmar, G. Kanisch, G. Vidmar, Appl. Radiat. Isot. **69** (6), 908–911 (2011).
- [44] J. F. Ziegler, Nucl. Instrum. Methods B **219**, 1027 (2004). <http://www.srim.org/>.
- [45] Siddharth Parashari, S. Mukherjee, A. P. Singh, Vibha Vansola, H. Naik, B. K. Nayak, Rajnikant Makwana, S. V. Suryanarayana, N. L. Singh, Mayur Mehta, Y. S. Sheela, M. Karkera, R. D. Chauhan and S. C. Sharma, Phys. Rev. C **98**, 014625 (2018).